Nuclear Instruments and Methods in Physics Research A 726 (2013) 1–7

Contents lists available at SciVerse ScienceDirect

Nuclear Instruments and Methods in Physics Research A

journal homepage: www.elsevier.com/locate/nima

Improved SPICE electrical model of silicon photomultipliers

D. Marano [a,*], G. Bonanno [a], M. Belluso [a], S. Billotta [a], A. Grillo [a], S. Garozzo [a], G. Romeo [a], O. Catalano [b], G. La Rosa [b], G. Sottile [b], D. Impiombato [b], S. Giarrusso [b]

[a] INAF, Osservatorio Astrofisico di Catania, Via S. Sofia 78, I-95123 Catania, Italy
[b] INAF, Istituto di Astrofisica Spaziale e Fisica Cosmica di Palermo, Via U. La Malfa 153, I-90146 Palermo, Italy

ARTICLE INFO

Article history:
Received 22 February 2013
Received in revised form
8 May 2013
Accepted 22 May 2013
Available online 29 May 2013

Keywords:
Electrical models
Equivalent circuits
Output pulses
Silicon photomultipliers
Transient waveforms

ABSTRACT

The present work introduces an improved SPICE equivalent electrical model of silicon photomultiplier (SiPM) detectors, in order to simulate and predict their transient response to avalanche triggering events. In particular, the developed circuit model provides a careful investigation of the magnitude and timing of the read-out signals and can therefore be exploited to perform reliable circuit-level simulations. The adopted modeling approach is strictly related to the physics of each basic microcell constituting the SiPM device, and allows the avalanche timing as well as the photodiode current and voltage to be accurately simulated. Predictive capabilities of the proposed model are demonstrated by means of experimental measurements on a real SiPM detector. Simulated and measured pulses are found to be in good agreement with the expected results.

1. Introduction

Silicon photomultipliers (SiPMs), also referred to as multi-pixel photon counters (MPPCs), are a contemporary rapidly developing class of solid-state detectors which have been gaining great interest and extensive diffusion in the fields of high-energy physics, nuclear medicine, and astrophysics.

SiPM photo-sensors consist of a parallel array of photodiodes (SPADs), connected in parallel and operating above their breakdown voltage. When an optical photon strikes one of the basic microcells, the related photodiode undergoes a Geiger avalanche and the released charge is collected onto a common electrode. The series quenching resistance integrated in each pixel slows the avalanche current by reducing the voltage drop across the diode terminals. When the current is quenched, the cell begins to recharge, recovering its preceding quiescent bias conditions. The peak amplitude of the SiPM output generated signal is directly proportional to the total number of microcells which is struck by optical photons [1–6].

The availability of an accurate electrical model can enrich understanding of the design and behaviour of the SiPM detector as a signal source, allowing a reliable interpretation of its static and dynamic characteristics and its physical interactions with the coupled front-end electronics.

This work develops a new truthful SPICE electrical model of the SiPM sensors based on the peculiar physical features of each SPAD microcell composing the detector structure. Compared to previously reported models, the proposed circuit configuration provides a more accurate representation of the trigger generation processes underlying the transient response of the optical device to an incoming avalanche event.

In Section 2 the novel SiPM electrical model is addressed. Simulation results are discussed in Section 3. Experimental validation of the proposed model is performed in Section 4. Finally, Section 5 summarizes the paper conclusions.

2. Proposed electrical model

The circuit electrical model which is typically associated to the single elementary SPAD microcell is illustrated in Fig. 1 [1–4].

The avalanche photodiode is modeled as a parallel connection between the internal resistance of the diode space-charge region R_d, and the junction capacitance of the inner depletion layer C_d. The integrated quenching resistance R_q is associated with its parallel stray capacitance C_q, and an additional parasitic capacitance C_m across the microcell terminals is also introduced to account for metal lines and bonding pads.

The above electrical model is easily extendable to the case when more than one microcell is fired by an avalanche event by connecting in parallel multiple SPAD elements.

Avalanche triggering is modeled by means of an ideal DC voltage supply V_{BD} with a series voltage-controlled switch S_0.

* Corresponding author. Tel.: +39 0957332213.
E-mail address: davide.marano@oact.inaf.it (D. Marano).

0168-9002/$ - see front matter © 2013 Elsevier B.V. All rights reserved.
http://dx.doi.org/10.1016/j.nima.2013.05.127

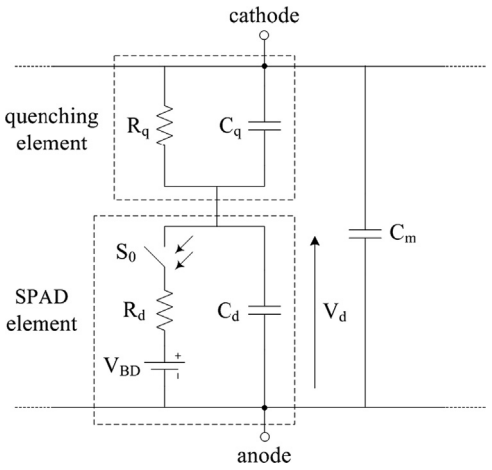

Fig. 1. Traditional equivalent electrical model of a single SPAD microcell.

The switch closes at a preset time t_{on}, demarking the start of a breakdown event, and a pulse current signal is then generated through the photodiode resistance R_d. When this current drops below a predefined threshold value I_{TH0}, the switch opens and the avalanche is quenched. The switch controlling voltage is realized by a square-wave source, whose pulse width T_{pw} represents the time between the avalanche triggering time t_{on} and the instant at which the decaying current decreases below the threshold level. Successively, the diode enters the recharging operation, and the transient voltage across its terminals slowly rises towards the external cathode voltage.

The time current and voltage waveforms $i_{Rd}(t)$ and $v_d(t)$, resulting from the SPAD model in Fig. 1 when closed to a load resistor R_L, are illustrated in Fig. 2 with relation to the external step-wise voltage $v_{ph0}(t)$, applied to the control switch and producing the trigger event. The current signal $i_{RL}(t)$ through the output load is also shown.

The main limitation of the conventional trigger generation approach derives from the statistical nature of the avalanche process. More specifically, the aleatory current amplitude I_{TH0} below which the avalanche is not able to self-sustain inevitably involves uncertainty on the choice of T_{pw} as the quenching time. As a result, the total charge Q_{TOT} in the avalanche pulse, which is strongly related to the diode quenching time, will be affected by the chosen value of T_{pw}. Most importantly, a constant switch timing in the microcells model does not allow a truthful representation of the output pulse waveforms as functions of the external operating voltage. Indeed, as the voltage $V_{OV} = V_K - V_{BD}$, better known as overvoltage or excess voltage, is increased from its nominal value, the potential across the photodiode is initially greater, and so a higher avalanche discharge current flows through the diode, which then takes a longer time to drop to the same quenching level. This entails an increased amplitude of the output pulses during the recovery operation with respect to those obtained with a constant switching time, with consequent simulation discrepancies on the overall pulse charges.

To overcome the above mentioned limitations and better relate the SiPM electrical model to the physics of the device, an improved circuit configuration is realized to provide an equal switch timing for all bias voltages, hence releasing the diode quenching time from the choice of the pulse width T_{pw} of the switch control voltage.

The proposed circuit model allows to optimize the control mechanism of the trigger event and make the internal quenching time independent of the external control voltage, thus providing reliable simulations of the charge collection as a function of the overvoltage.

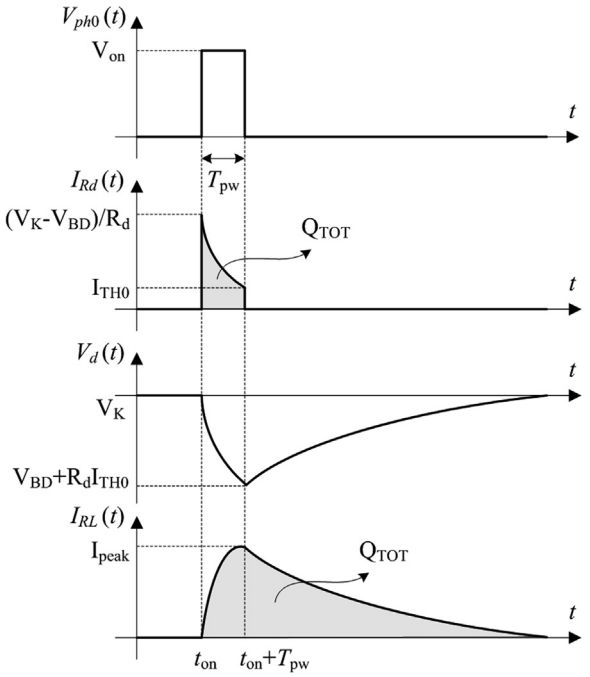

Fig. 2. Characteristic transient current, voltage and output signal waveforms resulting from the traditional SiPM single cell model in Fig. 1, with relation to the external switch control voltage simulating a detected event.

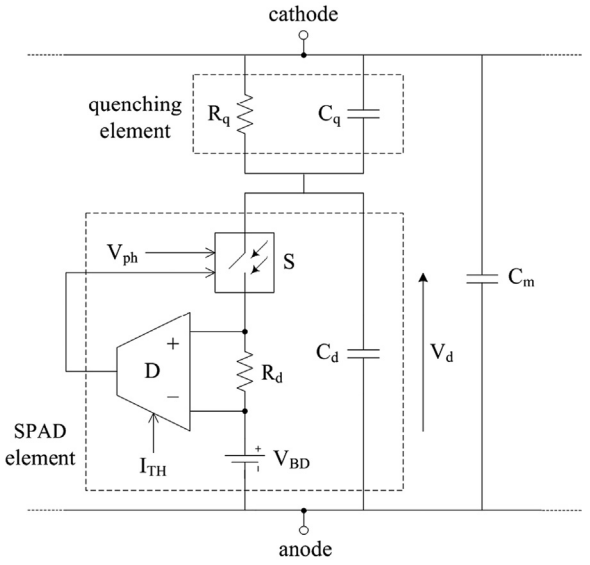

Fig. 3. Simplified block diagram of the improved equivalent electrical model of a single SPAD microcell.

Fig. 3 shows the simplified block diagram of the improved electrical model of each SiPM basic microcell. A voltage signal V_{ph} starts the trigger avalanche by closing the switch S. A negative feedback loop, including a discriminator D, monitors the diode current and acts upon the switch opening time when this current falls below the specified I_{TH} value.

The novel transient current and voltage waveforms for the improved model in Fig. 3, when closed to a load resistor R_L, are illustrated in Fig. 4. The switch control voltage, V_{ph}, can now be realized as a pulse-wave generator of arbitrary width. However, to perform a correct operation, the voltage pulse is required to have a smaller width compared to the quenching time. As a result of the modified single-cell model, although the threshold current level is

not sharply defined, the switch S always opens when the photodiode current reaches the constant value of I_{TH} for all operating voltages. In this way, the diode quenching time T_q is no more related to the switching voltage V_{ph}, and a more accurate representation of the charge collection is achieved.

3. Simulation results

SPICE circuit implementations of the conventional and improved electrical models in Figs. 1 and 3 are respectively depicted in Figs. 5 and 6, for a number N_f of active pixels over a total number of N microcells. The equivalent electrical model of the remaining $N-N_f$ parallel-connected cells is simply derived by eliminating the circuit branch composed by the V_{BD} voltage source and the photodiode equivalent resistance.

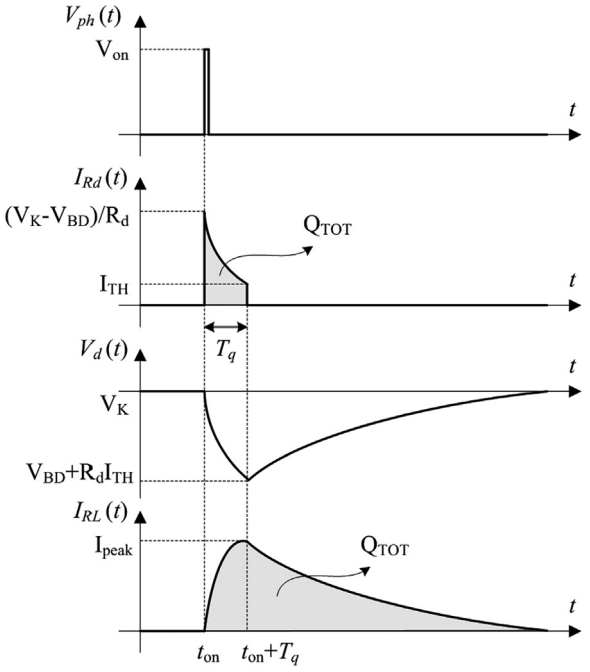

Fig. 4. Characteristic transient current, voltage and output signal waveforms resulting from the improved SiPM single cell model in Fig. 3, with relation to the external switch control voltage simulating a detected event.

The quenching time of the SiPM output pulses is assumed to be the instant at which the current through the equivalent photo diode resistance $R_{d\_eq}=R_d/N_f$ crosses the threshold level $I_{TH\_eq}=N_fI_{TH}$, established by the average quenching current of an individual microcell and by the number of firing cells.

Referring to the newly proposed SPICE model in Fig. 6, a couple of parallel voltage-controlled switches, S_1 and S_2, is exploited in series with the diode resistance and an open-loop operational amplifier is inserted in the feedback branch as a threshold discriminator to monitor the avalanche current transitions. The initial trigger generation is accomplished by S_2 through the input pulse signal V_{ph}.

In the steady-state operation, when no trigger events are detected, the voltage across the equivalent diode resistance is lower than the discriminator threshold $V_{TH}=R_dI_{TH}$, so that the negatively saturated amplifier output voltage opens the switch S_1 and no current flows in the circuit. When a positive pulse is applied to V_{ph}, the avalanche current instantaneously produces a voltage drop on R_{d_eq} which commutates the comparator output towards its positive saturation voltage, hence closing S_1 and guaranteeing the discharging current to keep on flowing regardless of S_2. As soon as the avalanche current reaches the equivalent threshold level, the discriminator turns again to its preceding state and opens S_1, thus collapsing the avalanche and determining the actual quenching time.

Fig. 7 reports the complete SiPM electrical model, showing the simulated values of the circuit parameters.

To confirm the different effects of increasing overvoltage on the pulse waveforms of the conventional and improved SiPM electrical models, Figs. 8 and 9 illustrate, respectively, the voltage across the photodiode and the current through the diode resistance for $N=3600$, $N_f=1$, and for three rising values of V_{OV}. As can be noted, with a constant switching time, the charge collected from the avalanche pulses does not increase with overvoltage as much as it raises in the improved electrical model. In particular, the increments in the total collected charge are found to be 70.36 fC and 140.65 fC, for the traditional model, and 80.92 fC and 162.15 fC, for the improved model, respectively. As a result, the amplitude of the SiPM output signal is also found to be slightly greater in the

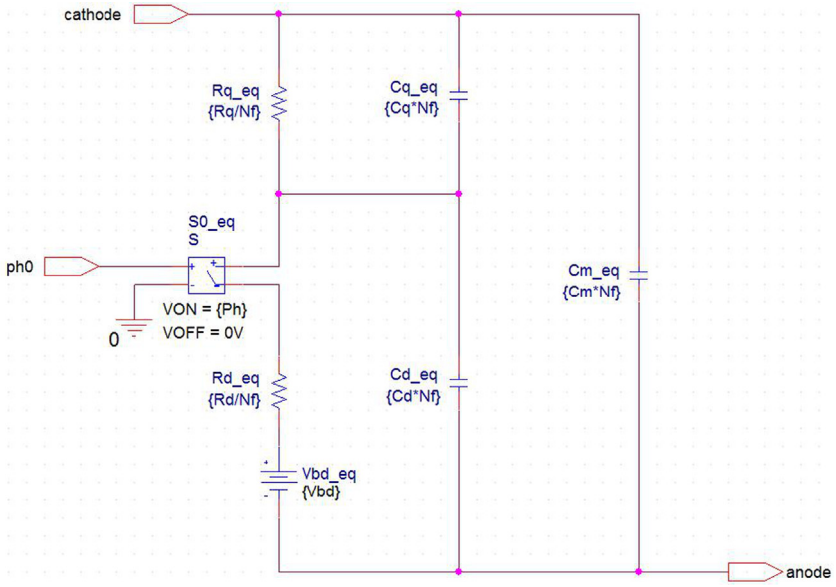

Fig. 5. Schematic of the typical electrical model of the SiPM active cells.

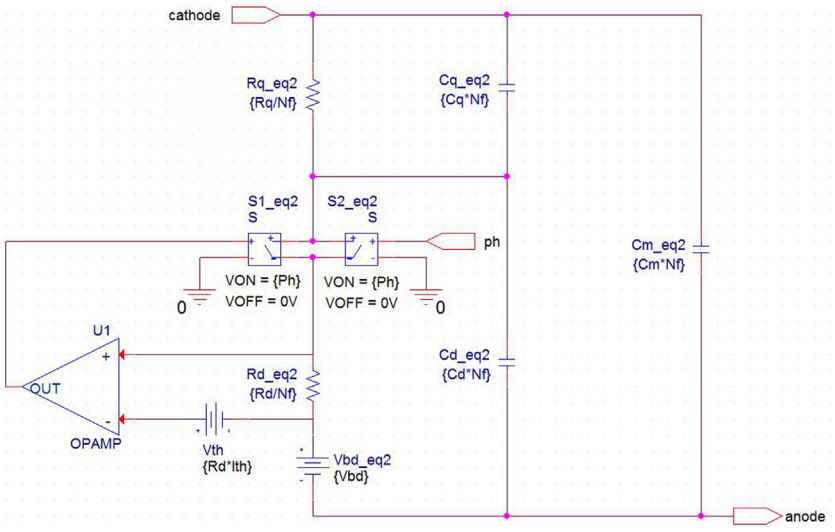

Fig. 6. Schematic of the improved electrical model of the SiPM active cells.

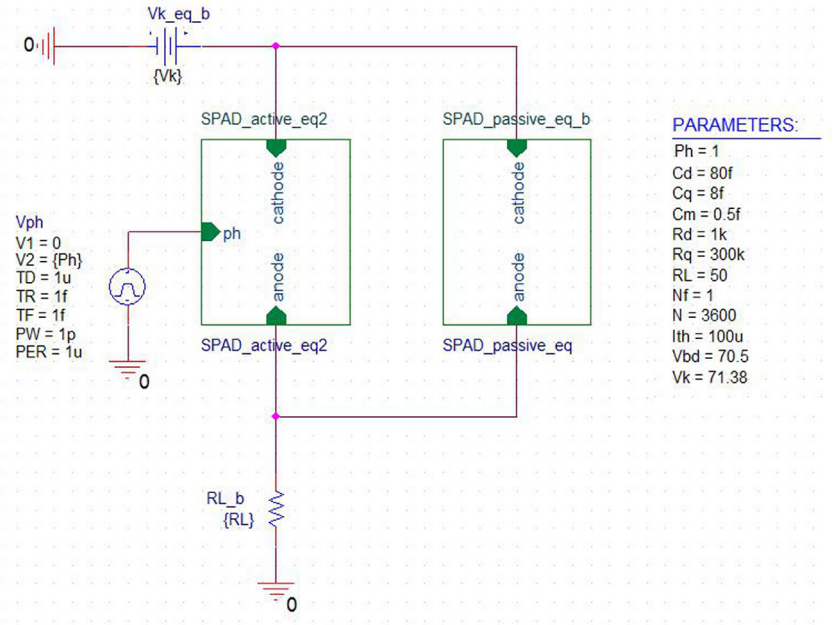

Fig. 7. Equivalent circuit of the overall SiPM architecture.

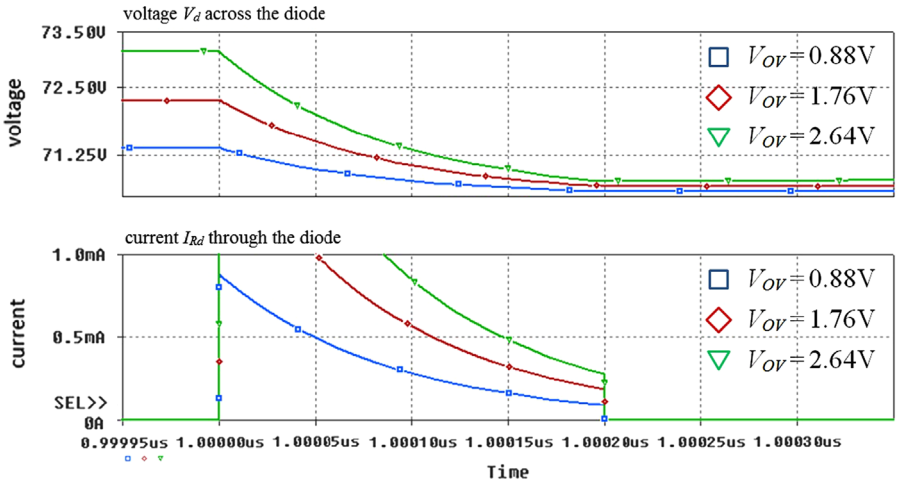

Fig. 8. Transient I_{Rd} and V_d waveforms of the conventional SiPM model, for $N=3600$, for a single fired cell ($N_f=1$), and for increasing values of V_{OV}. With a constant switch timing, the current in the diode stops at the same time instant for all bias voltages.

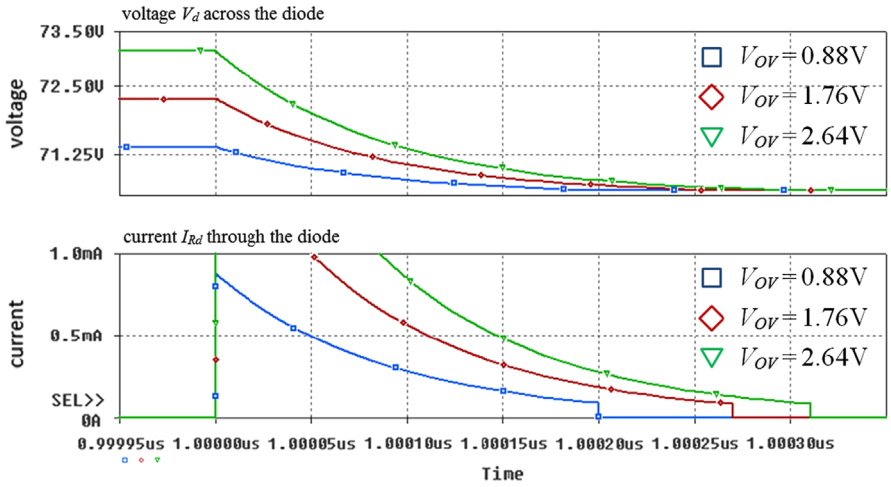

Fig. 9. Transient I_{Rd} and V_d waveforms of the improved SiPM model, for $N=3600$, for a single fired cell ($N_f=1$), and for increasing values of V_{OV}. With an optimized switch timing, the current in the diode stops when it reaches a constant value for all bias voltages.

proposed SPICE model, hence demonstrating a more truthful agreement with the physics of the device.

4. Experimental validation

Simulated and measured output pulse waveforms are compared together for a 3×3 mm^2 Hamamatsu MPPC device (S11828-3344MX) with a 50-μm pitch size. Measurements are performed at the Catania astrophysical Observatory Laboratory for Detectors (COLD).

A PDL 200B pulsed diode laser, emitting rays at a 405-nm wavelength, is used to produce the trigger avalanche into the MPPC microcells. The laser radiation intensity is controlled such that only a few cells get fired for each event. Pulse waveforms are acquired on a digital oscilloscope with a 2.5-GHz bandwidth, a 20-GS/s sampling rate, and an intrinsic 1-mV baseline noise.

The laser pulses are set to be significantly shorter than the detector response time. Moreover, the frequency of the laser source flux is sufficiently small to allow a full recovery transition between two subsequent trigger events.

A dedicated test-board for the MPPC device is specifically developed, shown in Fig. 10. It basically provides the multiple anodes connection of single MPPC pixels and allows the common cathode terminal to be connected to an external bias reference. An internal pre-amplifier is included in the top board for gain regulation and a band-gap sensor is also embedded to provide temperature measurements. An appropriate mechanical interface is additionally implemented in order to allow the laser light to shine upon the detector surface.

The detector unit under test is connected to the input of an SP5600 CAEN power/amplification system with a 50-Ω input resistance and a tunable-gain pre-amplifier.

For a fixed operating voltage, histograms of the maximum pulse amplitudes are digitally captured according to the number of cells firing for each event. Afterwards, events with the same number of fired cells are grouped together and averaged to form a single pulse waveform.

Experimental measures are also used to extract circuit parameter values as well as to validate the developed model.

Model parameters extraction is accomplished by means of an effective characterization procedure of the detector breakdown voltage, total microcell capacitance, and quenching and diode resistances. In particular, the photodiode resistances are obtained from the slope of the forward I–V static characteristics; the charge

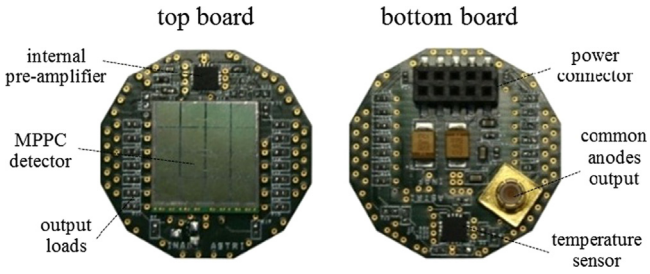

Fig. 10. Dedicated COLD test-board for the 3×3 mm^2 MPPC detector device.

delivered after a Geiger discharge is derived by applying a linear fit to the peak positions in a signal charge histogram; and the total microcell capacitance and breakdown voltage are respectively determined from the slope and x-axis intercept of the associated curve relating the measured charge to the external operating voltage. The extracted values for the 3×3 mm^2 Hamamatsu macro-pixel device are reported in Fig. 7.

Based on the obtained V_{BD}, the external bias voltage V_K is regulated in order to achieve an overvoltage $V_{OV}=1.3$ V, ensuring a Geiger-mode operation of the MPPC detector.

Simulated and experimental voltage waveforms are respectively plotted in Fig. 11 and in Fig. 12, for $N=3600$ and rising values of the fired cells. The simulated pulse functions refer to the improved SPICE model, and are scaled by considering a 36-dB pre-amplifier gain factor.

The pre-amplifier roughly shapes the original signal, due to its limited frequency bandwidth, so the curve peaks are consequently smoothed. However, the slowest part of the transient responses is in good accordance with the simulated waveforms. In particular, for a single firing cell, the normalized overall current pulse charge, calculated as the integral of the output voltage pulse divided by the load resistance, is found to be 6.9 pC for the modeled pulse waveform, while an average value of 7 pC is obtained from the relevant acquired signal. In addition, a good peak linearity is achieved for increasing values of the firing cells for both modeled and acquired pulses.

To further corroborate the effectiveness of the adopted model and achieve a more accurate comparison between the simulated and experimental pulse waveforms, the SPICE model of the CAEN voltage pre-amplifier is additionally included in the simulation model cascaded to the output load resistor, in order to account for the frequency limitation of the measured output signal. For a single firing cell, data outputs of the simulated and measured

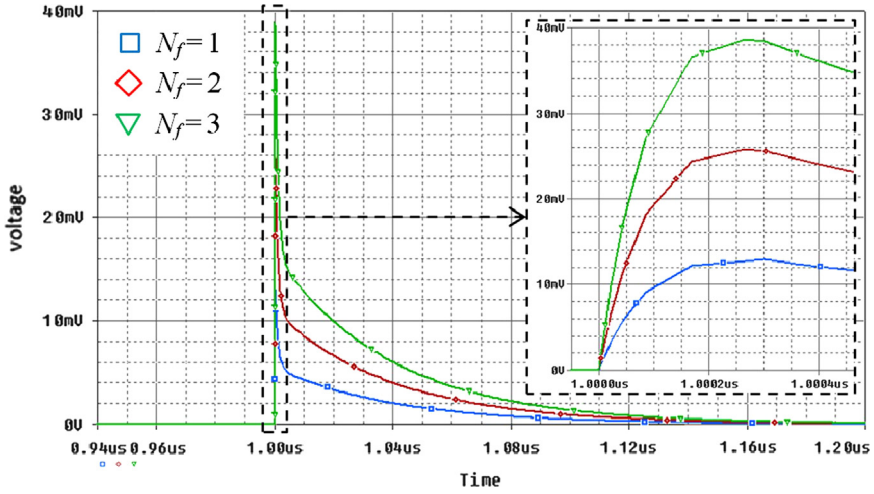

Fig. 11. Simulated pulse waveforms, for $N=3600$ and rising values of N_f.

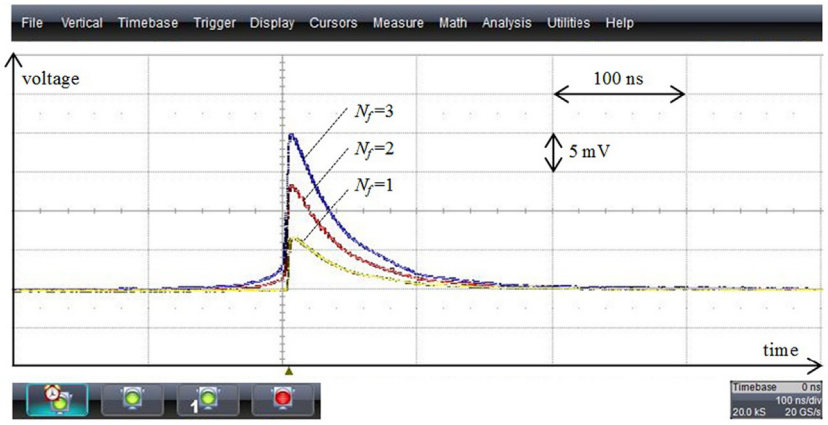

Fig. 12. Measured pulse waveforms, for $N=3600$ and rising values of N_f.

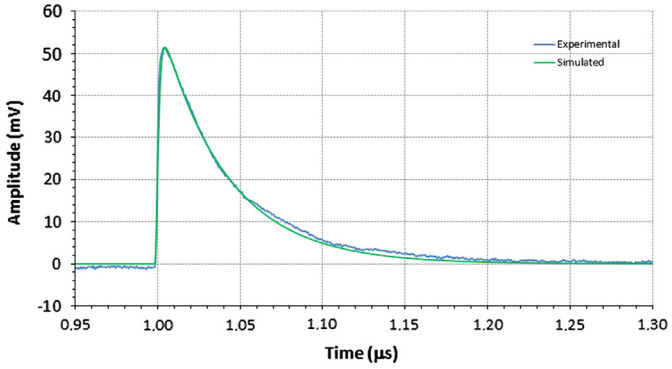

Fig. 13. Simulated and experimental output pulse waveform comparison, for $N=3600$ and a single firing cell.

pulses are merged together into a single plot; Fig. 13 shows the resulting pulse waveforms under a 1.3-V overvoltage and a 50-dB pre-amplifier gain.

From a direct inspection of the output curves, both simulated and measured waveforms are well-overlapped even during the fast phase of their transient responses. Thereby, the adopted model can also achieve a truthful reproduction of the shaping in the rising edge of the measured SiPM output signals.

5. Conclusions

A new accurate electrical model is developed to simulate, validate, and predict the output response of SiPM detectors. The adopted model allows for an accurate representation of the device behaviour. The trigger avalanche is simulated by means of a pair of parallel voltage-controlled switches, along with a negative feedback loop controlling current through the photodiode resistance. Model parameters values are extracted based on the experimental measurements performed. The adopted model has been successfully validated by comparing SPICE simulations to measured pulse waveforms obtained from a real SiPM device detector.

Acknowledgments

This work was partially supported by the ASTRI Flagship Project, financed by the Italian Ministry of Education, University, and Research (MIUR) and led by the Italian National Institute for Astrophysics (INAF).

References

[1] G. Condorelli, D. Sanfilippo, G. Valvo, M. Mazzillo, D. Bongiovanni, A. Piana, B. Carbone, G. Fallica, Nuclear Instruments and Methods in Physics Research Section A 654 (2011) 127.

[2] S. Cova, M. Ghioni, A. Lacaita, C. Samori, F. Zappa, Applied Optics 35 (12) (1996) 1959.
[3] S. Seifert, H.T. van Dam, J. Huizenga, R. Vinke, P. Dendooven, H. Lhner, D.R. Schaart, IEEE Transactions on Nuclear Science NS-56 (6) (2009) 3726.
[4] K.A. Wangerin, G.-C. Wang, C. Kim, Y. Danon, Passive electrical model of silicon photomultipliers, in: Proceedings of IEEE Nuclear Science Symposium Conference Record, 2008, pp. 1276–1280.
[5] F. Corsi, A. Dragone, C. Marzocca, A. Del Guerra, P. Delizia, N. Dinu, C. Piemonte, M. Boscardin, G.F. Dalla Betta, Nuclear Instruments and Methods in Physics Research Section A 572 (2007) 416.
[6] N. Pavlov, G. Mhlum, D. Meier, Gamma spectroscopy using a silicon photomultiplier and a scintillator, in: Proceedings of IEEE Nuclear Science Symposium Conference Record, 2005, pp. 173–180.